Semi-Passive 3D Positioning of Multiple RIS-Enabled Users

Kamran Keykhosravi, *Member, IEEE*,
Musa Furkan Keskin, *Member, IEEE*,
Satyam Dwivedi, *Member, IEEE*,
Gonzalo Seco-Granados, *Senior Member, IEEE*,
and Henk Wymeersch, *Senior Member, IEEE*

***Abstract*—Reconfigurable intelligent surfaces (RISs) are set to be a revolutionary technology in the 6th generation of wireless systems. In this work, we study the application of RIS in a multi-user passive localization scenario, where we have one transmitter (TX) and multiple asynchronous receivers (RXs) with known locations. Classical approaches fail in this scenario due to lack of synchronization and lack of data association between multi-static measurements and users. To resolve this, we consider each user to be equipped with an RIS, and show that we can avoid the data association problem and estimate users' 3D position with submeter accuracy in a large area around the transmitter, using time-of-arrival measurements at the RXs. We develop a low-complexity estimator that attains the corresponding Cramér-Rao bound as well as a novel RIS phase profile design to remove inter-path interference.**

***Index Terms*—Reconfigurable intelligent surfaces, passive localization, Cramér-Rao lower bounds.**

I. Introduction

Realization of smart radio environments empowered by reconfigurable intelligent surfaces (RISs), which enables ubiquitous communication and radio sensing with high energy and spectrum efficiency, is one of the ambitions of the sixth generation of wireless systems [1]. RIS consists of a multitude of unit cells, whose responses to the impinging electromagnetic wave can be controlled, and can thereby improve the quality and coverage of wireless communication and also enable or improve radio localization [2]–[6], where a fixed RIS with known location is used for improving localization [2]–[5] or radar sensing [6] performance. In addition to these benefits, RISs are semi-passive devices with low cost, which make them ideal to be mounted on surfaces as well as moving objects.

Manuscript received March 15, 2021; revised July 1, 2021; accepted August 26, 2021. Date of publication September 2, 2021; date of current version October 15, 2021. This work was supported in part by the Swedish Research Council under Grant 2018-03701, in part by the Marie Skłodowska-Curie Individual Fellowships (H2020-MSCA-IF-2019) under Grant 888913 (OTFS-RADCOM), in part by the Vinnova 5GPOS project under Grant 2019-03085, in part by the EU H2020 RISE-6G project under Grant 101017011, in part by the Spanish Ministry of Science, Innovation and Universities under Projects TEC2017-89925-R, and in part by the ICREA Academia Programme. The review of this article was coordinated by Dr. Boya Di. *(Corresponding author: Kamran Keykhosravi.)*

Kamran Keykhosravi, Musa Furkan Keskin, and Henk Wymeersch are with the Department of Electrical Engineering at Chalmers University of Technology, 41296 Gothenburg, Sweden (e-mail: kamrank@chalmers.se; furkan@chalmers.se; henkw@chalmers.se).

Satyam Dwivedi is with the Ericsson Research, 16440 Stockholm, Sweden (e-mail: satyam.dwivedi@ericsson.com).

Gonzalo Seco-Granados is with the Department of Telecommunications and Systems Engineering, Universitat Autónoma de Barcelona, 08029 Barcelona, Spain (e-mail: gonzalo.seco@uab.cat).

Digital Object Identifier 10.1109/TVT.2021.3109786

Radio localization has attracted increasing attention in recent years as technologies such as millimeter wave, multiple-input multiple-output (MIMO), and RIS enable high-accuracy positioning of users based on the time-of-arrival (ToA) and angles-of-arrival and -departure measurements [7]. To extract information from ToA measurements, periodic synchronization between the infrastructure nodes is necessary, which forms a bottleneck when sub-ns accuracy levels are required. Considering the nature of the user, localization techniques can be categorized into active and passive methods. While with the former case the user transmits or receives signals (e.g., in [7], where multipath was exploited to reduce the need for synchronization), in the latter case, the user only reflects or scatters the signals from a transmitter (TX) (see e.g., [8]). Many studies have been conducted on passive localization based on a variety of approaches such as radio-frequency identification (RFID) [9], [10], signal eigenvectors [8], received signal strength (RSS) [11], and ToA-based passive positioning [12]–[16]. In the latter case, which is the focus of this letter, the user location is estimated based on the received signal ToA at multiple receivers (RXs). Again synchronization is of importance, leading to studies in two-dimensional space under the assumption of synchronous [12], quasi-synchronous [13], and asynchronous networks [14]. Moreover, bistatic ToA estimation has been investigated in passive sensing systems that employ the signals transmitted by illuminators of opportunity (IO) [16]. An important challenge in these works is to perform data association, that is, to determine that which measurement correspond to which target. To address this, in [15] the 2D localization of a joint radar and RFID system was proposed.

In this work, we investigate the multi-user 3D passive positioning problem under multi-static and asynchronous setup. Due to the aforementioned synchronization and data association challenges, this is a fundamentally intractable localization problem. To render the problem solvable, each user is equipped with an RIS. We propose a low-complexity positioning algorithm, which utilizes orthogonal sequences in the design of RIS phase profiles, helping the algorithm to resolve multipath interference and the data association problem, which enables localization of the user equipments (UEs). We evaluate the localization error of the proposed method and show that it reaches the theoretical Cramér-Rao lower bounds (CRB). To the best our knowledge, this is the first paper on passive localization of RIS-enabled users, where the RISs are not part of the infrastructure and therefore have unknown locations.

Notation: Vectors, which are columns, are shown by bold lower-case letters and matrices by bold upper-case ones. The element at the ith row and the jth column of the matrix $\boldsymbol{A}$ is shown as $[\boldsymbol{A}]_{i,j}$. The sets $\mathbb{C}$ and $\mathbb{T}$ represents the set of complex numbers and all the complex numbers with unit magnitude, respectively. The vector $\mathbf{1}$ indicates the all-ones vector and the operator $\circ$ specifies the element-wise multiplication.

II. System Model

A. Signal Model

We consider one TX (a base station (BS)) with *known* location $\boldsymbol{p}_0$ and M RXs (BSs or road-side units) with *known* locations $\boldsymbol{p}_1, \ldots, \boldsymbol{p}_M$, as well as N UEs with *unknown* locations $\boldsymbol{x}_1, \ldots, \boldsymbol{x}_N$. Each of the UEs is equipped with an RIS, while the TX and RXs have a single antenna (the analysis and method also applies to TX and RXs with multiple antennas). The RXs are not synchronized with the BS and have *unknown* clock biases $B_1, \ldots, B_M$. Each RX receives the

0018-9545 © 2021 IEEE. Personal use is permitted, but republication/redistribution requires IEEE permission.
See https://www.ieee.org/publications/rights/index.html for more information.

Authorized licensed use limited to: Universitat Autonoma De Barcelona. Downloaded on July 19,2022 at 23:51:31 UTC from IEEE Xplore. Restrictions apply.

signal directly from the TX, which is the line-of-sight (LOS) path, and also the reflected (TX–RIS–RX) signals from RISs, which is the non line-of-sight (NLOS) path). We consider the transmission of T orthogonal frequency-division multiplexing (OFDM) symbols with K subcarriers during each localization occasion, where we assume that T is sufficiently small, i.e., the user movement during the transmission is much less than (e.g., 10%) the wavelength, so that the transmission takes place within the coherence time of the channel, which can be considered constant during that interval.

The signal received at the mth RX, after cyclic prefix removal and fast Fourier transform (FFT), can be represented by the matrix $\boldsymbol{Y}_m \in \mathbb{C}^{K\times T}$. Assuming constant pilot transmission over all subcarriers, we have (see for example [5])

$$\boldsymbol{Y}_m = \sqrt{E_{\rm s}}\left(\sum_{n=0}^{N}\boldsymbol{d}(\tau_{n,m})\boldsymbol{\alpha}_{n,m}^{\top}+\sum_{s=0}^{N_{\rm s}}\boldsymbol{d}(\nu_{s,m})\boldsymbol{\eta}_{s,m}^{\top}\right)+\boldsymbol{W}_m \quad (1)$$

where $E_{\rm s}$ is the symbol energy and

$$\boldsymbol{d}(\tau) = [1, e^{\jmath 2\pi\Delta f\tau}, \ldots, e^{\jmath 2\pi(K-1)\Delta f\tau}]^{\top} \quad (2)$$

represents the phase offset produced by the delay on each subcarrier, where Δf is the subcarrier spacing. For the LOS path ($n=0$), the delay is $\tau_{0,m} = \|\boldsymbol{p}_0 - \boldsymbol{p}_m\|/c + B_m/c$, in which the distance $\|\boldsymbol{p}_0 - \boldsymbol{p}_m\|$ is known and c is the speed of light. For the reflected paths ($n>0$), the delay is

$$\tau_{n,m} = \frac{\|\boldsymbol{p}_0 - \boldsymbol{x}_n\| + \|\boldsymbol{x}_n - \boldsymbol{p}_m\| + B_m}{c}. \quad (3)$$

The vector $\boldsymbol{\alpha}_{n,m} \in \mathbb{C}^{T\times 1}$ represents the complex gain of different paths. For $n=0$ (LOS) $\boldsymbol{\alpha}_{0,m} = \alpha_{0,m}\mathbf{1}_T$, where $\alpha_{0,m}$ indicates the LOS gain. For $n\neq 0$, we have

$$[\boldsymbol{\alpha}_{n,m}]_t = \gamma_{n,0}\gamma_{n,m}\boldsymbol{a}^{\top}(\boldsymbol{\theta}_{n,m})\boldsymbol{\Omega}_n[t]\boldsymbol{a}(\boldsymbol{\phi}_{n,0}) \quad (4)$$

in which $\gamma_{n,0}$ is the complex channel gain from the transmitter to UE n and $\gamma_{n,m}$ is the complex channel gain from UE n to receiver m. The noise matrix is represented by $\boldsymbol{W}_m \in \mathbb{C}^{K\times T}$, which has i.i.d circularly-symmetric Gaussian elements and variance N_0. Moreover, $\boldsymbol{a}(\boldsymbol{\theta}_{n,m})$ is the steering vector as a function of the angle-of-departure (AoD) ($\boldsymbol{\theta}_{n,m}$) from the nth UE to the mth RX, and $\boldsymbol{\phi}_{n,0}$ is the angle-of-arrival (AoA) from the TX to the nth UE. Here, both angles are expressed in the frame of reference of the nth UE, which does not need to be known for our method to work. Let $\boldsymbol{R}_n$ indicate the unknown rotation matrix mapping the global frame of reference to the coordinate system associated with the nth RIS. Then AoD $\boldsymbol{\theta}_{n,m}$ represents the angle in the direction of vector $\boldsymbol{w}_{n,m} = \boldsymbol{R}_n(\boldsymbol{p}_m - \boldsymbol{x}_n)$, i.e., $[\boldsymbol{\theta}_{n,m}]_{\rm az} = \operatorname{atan2}([\boldsymbol{w}_{n,m}]_2, [\boldsymbol{w}_{n,m}]_1)$ and $[\boldsymbol{\theta}_{n,m}]_{\rm el} = \operatorname{acos}([\boldsymbol{w}_{n,m}]_3/\|\boldsymbol{w}_{n,m}\|)$. Similarly, $\boldsymbol{a}(\boldsymbol{\phi}_{0,n})$ indicates the nth RIS steering vector at AoA ($\boldsymbol{\phi}_{0,n}$) from the TX to the nth RX, which is the angle associated with the vector $\boldsymbol{v}_{n,0} = \boldsymbol{R}_n(\boldsymbol{p}_0 - \boldsymbol{x}_n)$. The steering vector at angle $\boldsymbol{\psi}$ for an RIS with $W_{\rm r}\times W_{\rm c}$ elements on the $x-y$ plane in the RIS coordinate system and distance d between adjacent elements is $\boldsymbol{a}(\boldsymbol{\psi}) = \boldsymbol{a}_{\rm r}(\boldsymbol{\psi})\otimes\boldsymbol{a}_{\rm c}(\boldsymbol{\psi})$, where

$$\boldsymbol{a}_{\rm r}(\boldsymbol{\psi}) = e^{\jmath\beta_{\rm r}}[1, e^{\jmath d[\boldsymbol{k}(\boldsymbol{\psi})]_1}, \ldots, e^{\jmath(W_{\rm r}-1)d[\boldsymbol{k}(\boldsymbol{\psi})]_1}]^{\top} \quad (5)$$

$$\boldsymbol{a}_{\rm c}(\boldsymbol{\psi}) = e^{\jmath\beta_{\rm c}}[1, e^{\jmath d[\boldsymbol{k}(\boldsymbol{\psi})]_2}, \ldots, e^{\jmath(W_{\rm c}-1)d[\boldsymbol{k}(\boldsymbol{\psi})]_2}]^{\top} \quad (6)$$

where $\beta_{\rm r} = -(W_{\rm r}-1)d[\boldsymbol{k}(\boldsymbol{\psi})]_1/2$ and $\beta_{\rm c} = -(W_{\rm c}-1)d[\boldsymbol{k}(\boldsymbol{\psi})]_2/2$ and

$$\boldsymbol{k}(\boldsymbol{\psi}) = \frac{2\pi}{\lambda}[\sin\psi_{\rm el}\cos\psi_{\rm az}, \sin\psi_{\rm el}\sin\psi_{\rm az}, \cos\psi_{\rm el}]^{\top} \quad (7)$$

is the wavenumber vector. The elevation angle is measured from the z axis and the azimuth angle in the $x-y$ plane from the x axis. We note that the AoAs, AoDs, and the user orientations are introduced to describe the channel model but they are not used in our estimation method. The phase profile of RIS at time t is indicated by the diagonal matrix $\boldsymbol{\Omega}_n[t] \in \mathbb{C}^{W\times W}$, where $W = W_{\rm r}W_{\rm c}$. Finally, the second summation in (1) models the effects of scatterers, where $N_{\rm s}$ is the number of scatterers, $\nu_{s,m}$ is the time delay associated with the sth scatterer, and $\boldsymbol{\eta}_{s,m} = \eta_{s,m}\mathbf{1}_T$, where $\eta_{s,m}$ captures the path loss from TX to the sth scatterer to the m-th RX. We derive the CRBs and the algorithm assuming $N_{\rm s}=0$, while we evaluate the performance for $N_{\rm s}\geq 0$.

B. Problem Formulation

Our goal is to estimate the locations of the N UEs, $\boldsymbol{x}_1, \ldots, \boldsymbol{x}_N$ from $\{Y_m\}_{m=1}^{M}$ in (1). To do this, we propose the following approach.

- To estimate at RX m, the $N+1$ ToAs $\tau_{n,m}$. For this, we use the design freedom of the RIS in terms of $\boldsymbol{\Omega}_n[t]$ to avoid interference from different paths.
- To compute time-difference-of-arrival (TDoA) measurements at each of the M RXs and process them jointly to localize all users.

III. Methodology

In this section, we address the two steps mentioned in Section II-B. We first introduce a special RIS phase profile design in Section III-A that allows us to decouple the received signals at each RX. Then based on the received signals we estimate ToAs in Section III-B. Finally, in Section III-C, we use the ToAs to estimate the position of the UEs.

A. RIS Phase Profile Design

We design the phase profile of each RIS to avoid the interference between different signal paths. To do so, for UE n, we set the RIS profile $\boldsymbol{\Omega}_n[t]$ to be the product between a constant diagonal matrix $\boldsymbol{\Omega}_n \in \mathbb{C}^{W\times W}$ and a time-varying scalar $[\boldsymbol{\omega}_n]_t \in \mathbb{T}$, i.e., $\boldsymbol{\Omega}_n[t] = [\boldsymbol{\omega}_n]_t\boldsymbol{\Omega}_n$, $t\in\{1,\ldots,T\}$. We also define $\boldsymbol{\omega}_0 = \mathbf{1}_T$, without loss of generality. As will be shown in Section III-B, we can avoid inter-path interference if the vectors $\boldsymbol{\omega}_n \in \mathbb{T}^{T\times 1}$ for $n=0,1,\ldots,N$ form an orthogonal set, i.e.,

$$\boldsymbol{\omega}_n^H\boldsymbol{\omega}_{n'} = \begin{cases} T & \text{if } n=n' \\ 0 & \text{otherwise.}\end{cases} \quad (8)$$

Therefore, one should set T higher than N to be able to select $N+1$ orthogonal vectors $\{\boldsymbol{\omega}_n\}_{n=0}^{N}$. We choose the vector $\boldsymbol{\omega}_n$ to be the nth column of the $T\times T$ discrete Fourier transform (DFT) matrix $\boldsymbol{F}$ with elements $[\boldsymbol{F}]_{\ell,m} = e^{-2\jmath\pi\ell m/T}$. Then, (8) holds since the columns of DFT matrices are mutually orthogonal. Here, we assume infinite resolution for the phase shifts of the RIS unit cells. For the case of limited RIS phase resolution, one can select $\{\boldsymbol{\omega}_n\}_{n=0}^{N}$ based on Butson-type Hadamard matrices [17].

In terms of the constant part $\boldsymbol{\Omega}_n$, since we do not assume any prior knowledge of the user location and orientation, we set this part randomly. However, if an initial estimation of the user location and orientation is available, one can design $\boldsymbol{\Omega}_n$ to obtain a higher signal-to-noise ratio (SNR) at the RXs.

Authorized licensed use limited to: Universitat Autonoma De Barcelona. Downloaded on July 19,2022 at 23:51:31 UTC from IEEE Xplore. Restrictions apply.

B. ToA Estimation At RX m

In order to estimate $\tau_{n,m}$ at RX m and for $n = 0 \dots N$, we make use of (8) by computing

$$\boldsymbol{r}_{n,m} = \frac{1}{T}\boldsymbol{Y}_m \boldsymbol{\omega}_n^* = \sqrt{E_\mathrm{s}}\beta_{n,m}\boldsymbol{d}(\tau_{n,m}) + \boldsymbol{z}_{n,m} \tag{9}$$

where $\boldsymbol{z}_{n,m} = \boldsymbol{W}_m \boldsymbol{\omega}_n^*/T$ and it can be shown that $\mathbb{E}\{\boldsymbol{z}_{n,m}\boldsymbol{z}_{n,m}^H\} = N_0/T\boldsymbol{I}$. Also,

$$\beta_{n,m} = \begin{cases} \alpha_{0,m} & \text{if } n = 0 \\ \gamma_{0,n}\gamma_{m,n}\boldsymbol{a}(\boldsymbol{\theta}_{m,n})^\top \boldsymbol{\Omega}_n \boldsymbol{a}(\boldsymbol{\phi}_{0,n}) & \text{otherwise.} \end{cases} \tag{10}$$

From this observation, we can easily determine $\tau_{n,m}$ using standard methods. Here, we use FFT with a refinement step based on quasi-Newton method [5]. We explain this method in brief for completeness. Upon receiving vector $\boldsymbol{r}_{n,m}$, we calculate $\boldsymbol{r}_{n,m}(\delta) = \boldsymbol{r}_{n,m} \circ \boldsymbol{d}(\delta)$, which mimics a delayed version of $\boldsymbol{r}_{n,m}$ in the frequency domain. Let $\boldsymbol{b}_{n,m}(\delta)$ be the F-point FFT of the vector $\boldsymbol{r}_{n,m}(\delta)$, where F is a design parameter. Then we estimate $\tau_{n,m}$ as $\hat{\tau}_{n,m} = \tilde{k}/(F\Delta f) - \tilde{\delta}$, where $[\tilde{\delta}, \tilde{k}] = \arg\max_{k,\delta} |[\boldsymbol{b}_{n,m}(\delta)]_k|$ and $\delta \in [0, 1/(F\Delta f)]$. This 2D optimization can be divided to two 1D ones [5].

C. Estimating the Position of User n

We compute the TDoA measurements

$$\Delta_{n,m} = c(\hat{\tau}_{n,m} - \hat{\tau}_{0,m}) + \|\boldsymbol{p}_0 - \boldsymbol{p}_m\| \tag{11}$$

$$= \|\boldsymbol{p}_0 - \boldsymbol{x}_n\| + \|\boldsymbol{x}_n - \boldsymbol{p}_m\| + w_{n,m}, \tag{12}$$

where we use the LOS paths as references to remove the clock biases B_m. Eq (12) defines an ellipsoid in 3D with foci $\boldsymbol{p}_0$ and $\boldsymbol{p}_m$. For each UE n, we aggregate all the measurements in $\boldsymbol{\Delta}_n = [\Delta_{n,1}, \dots, \Delta_{n,M}]^\top$ across different RXs and the corresponding noises in $\boldsymbol{w}_n$, where we model $\boldsymbol{w}_n \sim \mathcal{N}(\boldsymbol{0}, \boldsymbol{\Sigma}_n)$. Note that $\boldsymbol{\Sigma}_n$ is a diagonal matrix (which is different from the standard TDoA localization system), since the noises at different RXs are uncorrelated. The elements of $\boldsymbol{\Sigma}_n$ can be estimated using the CRB for $\tau_{n,m}$, which can be calculated based on [18, Chapter 3] (see also [7]) as

$$\mathrm{E}\left(|\tau_{n,m} - \hat{\tau}_{n,m}|^2\right) \geq \frac{6N_0}{K(K^2-1)TE_\mathrm{s}|2\pi\Delta f \beta_{n,m}|^2}. \tag{13}$$

Then based on (11), the covariance matrix $\boldsymbol{\Sigma}_n$ can be calculated as

$$[\boldsymbol{\Sigma}_n]_{m,m} = c^2\left(\mathrm{E}\left(|\tau_{n,m} - \hat{\tau}_{n,m}|^2\right) + \mathrm{E}\left(|\tau_{0,m} - \hat{\tau}_{0,m}|^2\right)\right) \tag{14}$$

where in order to calculate (13) we estimate $|\beta_{n,m}|$ based on (9) as

$$|\hat{\beta}_{n,m}| = \left|\frac{\boldsymbol{d}(\hat{\tau}_{n,m})^\top \boldsymbol{r}_{n,m}}{\sqrt{E_\mathrm{s}}\boldsymbol{d}(\hat{\tau}_{n,m})^\top \boldsymbol{d}(\hat{\tau}_{n,m})}\right|. \tag{15}$$

We introduce $\boldsymbol{\Delta}_n = \boldsymbol{h}(\boldsymbol{x}_n) + \boldsymbol{w}_n$, where $[\boldsymbol{h}(\boldsymbol{x})]_m = \|\boldsymbol{p}_0 - \boldsymbol{x}\| + \|\boldsymbol{x} - \boldsymbol{p}_m\|$. We thus find the UE location estimate as

$$\hat{\boldsymbol{x}}_n = \arg\min_{\boldsymbol{x}_n} (\boldsymbol{\Delta}_n - \boldsymbol{h}(\boldsymbol{x}_n))^\top \boldsymbol{\Sigma}_n^{-1} (\boldsymbol{\Delta}_n - \boldsymbol{h}(\boldsymbol{x}_n)) \tag{16}$$

which can be solved via gradient descent algorithm, starting from an initial guess. We now propose a method to find such an initial guess.

Without loss of generality, we set $\boldsymbol{p}_0 = \boldsymbol{0}$. In the absence of noise and based on (12), we have that $(\Delta_{n,m} - \|\boldsymbol{x}_n\|)^2 = \|\boldsymbol{x}_n - \boldsymbol{p}_m\|^2$, which leads to

$$\boldsymbol{p}_m^\top \boldsymbol{x} - \Delta_{n,m}\|\boldsymbol{x}_n\| = \frac{1}{2}(\|\boldsymbol{p}_m\|^2 - \Delta_{n,m}^2). \tag{17}$$

TABLE I
PARAMETERS USED IN THE SIMULATION

Parameter	Symbol	Value
Wavelength	λ	1 cm
RIS element spacing	d	0.5 cm
Light speed	c	3×10^8 m/s
Number of subcarriers	K	100
Subcarrier bandwidth	Δf	120 kHz
Number of transmissions	T	32
Transmission Power	$KE_\mathrm{s}\Delta f$	25 dBm
Noise PSD	N_0	-174 dBm/Hz
UE's Noise figure	n_f	5 dB
FFT dimensions	F	1024

We can rewrite (17) in the matrix form as $\boldsymbol{P}\boldsymbol{x}_n = \boldsymbol{z}_n + \boldsymbol{\Delta}_n\|\boldsymbol{x}_n\|$, where $\boldsymbol{P} = [\boldsymbol{p}_1, \boldsymbol{p}_2, \dots, \boldsymbol{p}_M]^\top, \boldsymbol{z} = 0.5[\|\boldsymbol{p}_1\|^2 - \Delta_{n,1}^2, \dots, \|\boldsymbol{p}_M\|^2 - \Delta_{n,M}^2]^\top$. Then the nth user position can be estimated as [19] $\hat{\boldsymbol{x}}_n = \boldsymbol{a}_n + \boldsymbol{b}_n\|\hat{\boldsymbol{x}}_n\|$, where $\boldsymbol{a}_n = (\boldsymbol{P}^\top\boldsymbol{P})^{-1}\boldsymbol{P}^\top\boldsymbol{z}_n$, $\boldsymbol{b}_n = (\boldsymbol{P}^\top\boldsymbol{P})^{-1}\boldsymbol{P}^\top\boldsymbol{\Delta}$, and

$$\|\hat{\boldsymbol{x}}_n\| = \frac{-\boldsymbol{a}_n^\top\boldsymbol{b}_n \pm \sqrt{(\boldsymbol{a}_n^\top\boldsymbol{b}_n)^2 - \|\boldsymbol{a}_n\|^2(\|\boldsymbol{b}_n\|^2 - 1)}}{\|\boldsymbol{b}_n\|^2 - 1}. \tag{18}$$

If (18) yields two viable solutions, one can insert both solutions to the negative log-likelihood function, which is the objective function in (16). If the outcome for one of the solutions is much smaller than the other one, then it should be used as the initial guess for the nth user position. However, if both outcomes are small, this indicates that the M ellipsoids in (12) intersect in two distinct points. In such a case some prior knowledge (e.g., the user is located in a given region in relation to the RXs) should be used to localize the user.

IV. SIMULATION RESULTS

In this section, we evaluate the proposed method. The RIS is a 256×256 uniform planar array (UPA). The clock biases B_m are selected uniformly in the interval $[0, 1/\Delta f)$. Since there is no interference between the LOS path and the NLOS paths from different users, the performance of the estimator for each user is independent of the number of users N (as long as $T > N$) and therefore, we set $N = 1$. For the LOS path, the channel gain $\alpha_{0,m}$ is calculated based on Friisâ formula assuming unit directivity for TX and RXs. For the NLOS path the channel gain is calculated as [20, Eq. (21)–(23)]

$$\gamma_{n,0}\gamma_{n,m} = \frac{\lambda^2(\cos(\theta_{n,m})\cos(\phi_{n,0}))^{0.285}}{16\pi\|\boldsymbol{p}_0 - \boldsymbol{x}_n\|\|\boldsymbol{p}_m - \boldsymbol{x}_n\|}. \tag{19}$$

All the rotational angles corresponding to the user orientation is set to zero ($\boldsymbol{R}_n = \boldsymbol{I}_3, \ \forall n$). The diagonal elements of $\boldsymbol{\Omega}_n$ are drawn randomly and independently from the unit circle. The presented results are obtained by averaging over 10,000 random realization of RIS phase profiles (100) and noise (100 for each RIS phase profile). In our estimator, we use the prior knowledge that the UE is below the RXs to resolve the sign ambiguity in (18). The rest of the system parameters are represented in Table I. To evaluate the performance of our estimator, we use PEB, which based on [18, Eq.(3.31)] and (12) can be calculated as $\mathrm{PEB}_n = \sqrt{\mathrm{tr}(\boldsymbol{J}_n^{-1})}$. Here, $\boldsymbol{J}_n = \dot{\boldsymbol{\mu}}_n\Sigma_n^{-1}\dot{\boldsymbol{\mu}}_n$ and

$$[\dot{\boldsymbol{\mu}}_n]_m = \frac{\boldsymbol{x}_n - \boldsymbol{p}_0}{\|\boldsymbol{x}_n - \boldsymbol{p}_0\|} + \frac{\boldsymbol{x}_n - \boldsymbol{p}_m}{\|\boldsymbol{x}_n - \boldsymbol{p}_m\|}. \tag{20}$$

In Fig. 1 the position error has been analyzed for a system with the TX at the origin, $M = 3$ RXs located on a circle with radius $R = 10$ m on the plane $z = 1$ m, and a user located on $z = -3$ m. Fig. 1(a) illustrates

Authorized licensed use limited to: Universitat Autonoma De Barcelona. Downloaded on July 19,2022 at 23:51:31 UTC from IEEE Xplore. Restrictions apply.

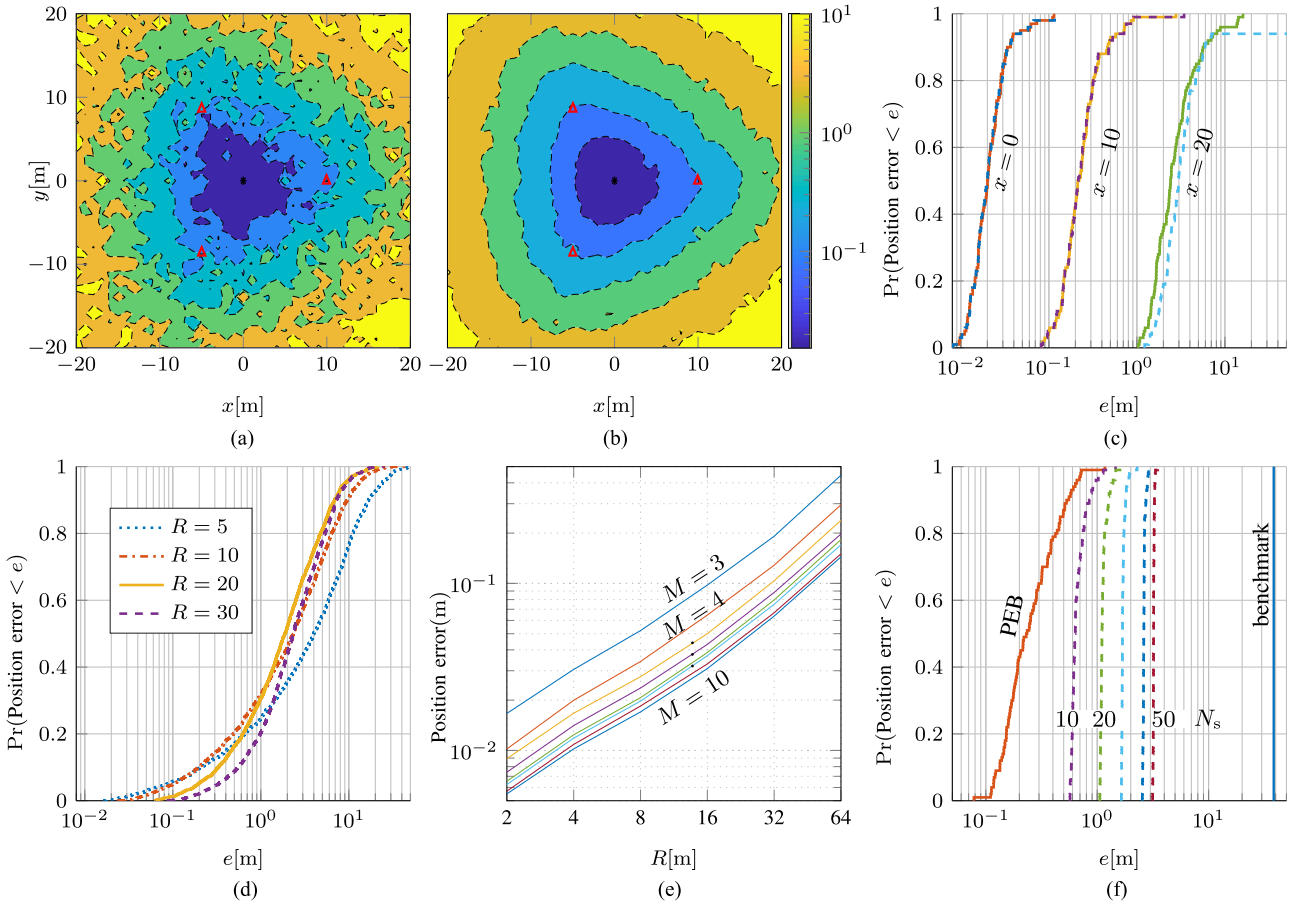

Fig. 1. The position error (in meters) for a system with one TX at the origin (marked by a black circle), $M = 3$ RXs (marked by red triangles) uniformly located on a circle with radius $R = 10$ on the plane $z = 1$, and a user located on $[x, y, -3]$: (a) position error bound (PEB) for one random RIS configurations; (b) the average of PEB over 100 random RIS configurations; (c) the CDF of PEB (solid lines) and estimation error (dashed lines) for 100 random RIS configurations at $[x, 0, -3]$ $x \in \{0, 10, 20\}$ meters; (d) the CDF of average PEB for 41×41 equispaced user locations shown in subfigure (a) with $R \in \{5, 10, 20, 30\}$; (e) average PEB at $[0, 0, -3]$ meters for $M = 3 \ldots 10$; (f) average PEB (solid line) and the estimation error (dashed lines) for 100 random RIS configurations at $[10, 0, -3]$ meters in the presence of $10, 20, 30, 40$, and 50 scatterers. Furthermore, as a benchmark, we present the PEB when RISs are replaced by single-element tags.

the PEB for one realization of the RIS phase profile while Fig. 1(b) does so for the average of the PEB over 100 random RIS configurations. It is evident that submeter localization accuracy can be attained in a large area around the TX. From Fig. 1(b) one can see that the average PEB gradually and symmetrically increases with the distance from the TX. In general, the same behavior can be observed also in Fig. 1(a), however, the increase in PEB is not smooth and symmetrical, which is due to different RIS reflection gains in different directions for a random phase profile. Fig. 1(c) represents the cumulative distribution function (CDF) of the PEB and the estimation error for 100 RIS configurations at three points. It can be seen that the presented estimator tightly attains the the PEB as long as the PEB is less than 8 meters.

In Fig. 1(d) we study the effect of RX placement on the average PEB. To do so, we evaluate the CDF of the average PEB for a 41 grid of UE locations over the area shown in Fig. 1(a). We consider four different values for the horizontal distance from RX to TX (R). It can be seen that for the majority of UE locations $R = 20$ m obtains superior position accuracy. This indicates that RXs should be placed close to the edge of the region of interest to improve the (worst-case) localization accuracy.

In Fig. 1(e) the PEB at a UE position equal to $[0, 0, -3]$ is calculated for different RX numbers (M) and positions (R) of receivers. It can be seen that PEB increases with R linearly, which is due to the quadratic decrease of SNR. Furthermore, it is evident that the improvement in PEB achieved by increasing the number of RXs is noticeable only for low values of M.

Fig. 1(f) illustrates the PEB and the estimation error at the UE position $[10, 0, -3]$ for 100 realizations of RIS configuration in the presence of additional scatterers. The scatterers are placed randomly one meter below the UEs and within 10 m radius of the point $[0, 0, -4]$. Since the scatterers are below the RIS, they only scatter the signal coming directly from the TX onto them and not the reflected signals from the RISs. The channel gain for the scattered signal (η_s) is calculated based on the radar range equation by assuming radar cross section of $0.1\,\mathrm{m}^2$. The interference from the scatterers deteriorates our estimation accuracy of the LOS delay $\hat{\tau}_{0,m}$, however, it does not affect that of the NLOS delay $\hat{\tau}_{n,m}$ $(n > 0)$. This is because the interference from scatterers cancels out upon calculating $\boldsymbol{r}_{n,m} = (1/T)\boldsymbol{Y}_m\boldsymbol{\omega}_n^*$ since we have $\mathbf{1}_T^\top \boldsymbol{\omega}_n^* = 0, \forall n > 0$. With a large number of scatterers, the position error is mainly affected by the error in LOS ToA estimation and therefore is predominantly independent of RIS phase profile, hence the sharp transition of CDF. We note that the estimator can perform properly even in the presence of a large number of scatterers. Finally, as a benchmark, we use a single-element reflector with 1 bit of phase resolution to emulate an RFID-like tag. The tag can then be used to eliminate the interpath interference [9]. It can be seen in Fig. 1(f) that the accuracy of the proposed method is much higher than that of the

Authorized licensed use limited to: Universitat Autonoma De Barcelona. Downloaded on July 19,2022 at 23:51:31 UTC from IEEE Xplore. Restrictions apply.

benchmark, which is due to the higher SNR caused by the multitude of RIS elements. This is achieved despite the fact that no prior knowledge of AoAs and AoDs are assumed and therefore RIS phase profiles are set randomly.

V. Conclusion

We considered a multi-user RIS-enabled localization problem, where the users' position in 3D was estimated by calculating the ToA of the LOS and NLOS paths at multiple receivers. The considered scenario can be categorized as a passive localization problem since the users do not generate transmitted signal or process received signals, but only reflect signals, based on which their positions are obtained. Nonetheless, it should be noted that RISs are not completely passive as they require some source of energy to reconfigure. We showed that by dividing the RIS phase profile to constant and time-varying parts and selecting the time-varying one based on orthogonal sequences, the interference between all the reflected NLOS signals among themselves and with the LOS paths can be avoided. Several extensions of this work are possible, e.g., RIS phase profile optimization to improve the SNR, exploitation of Doppler shifts to estimate the UEs velocities, and practical demonstration of the concept.

Acknowledgment

The authors gratefully acknowledge contributions of Jonas Medbo in seeding the idea of this article.

References

[1] D. Dardari, "Communicating with large intelligent surfaces: Fundamental limits and models," *IEEE J. Select. Areas Commun.*, vol. 38, no. 11, pp. 2526–2537, Nov. 2020.

[2] H. Wymeersch, J. He, B. Denis, A. Clemente, and M. Juntti, "Radio localization and mapping with reconfigurable intelligent surfaces: Challenges, opportunities, and research directions," *IEEE Veh. Technol. Mag.*, vol. 15, no. 4, pp. 52–61, Dec. 2020.

[3] H. Zhang, H. Zhang, B. Di, K. Bian, Z. Han, and L. Song, "Towards ubiquitous positioning by leveraging reconfigurable intelligent surface," *IEEE Commun. Lett.*, vol. 25, no. 1, pp. 284–288, Jan. 2021.

[4] A. Ranjha and G. Kaddoum, "URLLC facilitated by mobile UAV relay and RIS: A joint design of passive beamforming, blocklength, and UAV positioning," *IEEE Internet Things J.*, vol. 8, no. 6, pp. 4618–4627, Mar. 2021.

[5] K. Keykhosravi, M. F. Keskin, G. Seco-Granados, and H. Wymeersch, "SISO RIS-enabled joint 3D downlink localization and synchronization," in *Proc. IEEE Int. Conf. Commun.*, Montreal, QC, Canada, 2021, pp. 1–6.

[6] H. Zhang *et al.*, "Metaradar: Indoor localization by reconfigurable metamaterials," *IEEE Trans. Mobile Comput.*, to be published, doi: 10.1109/TMC.2020.3044603.

[7] A. Shahmansoori, G. E. Garcia, G. Destino, G. Seco-Granados, and H. Wymeersch, "Position and orientation estimation through millimeter-wave MIMO in 5G systems," *IEEE Trans. Wireless Commun.*, vol. 17, no. 3, pp. 1822–1835, Mar. 2018.

[8] J. Hong and T. Ohtsuki, "Signal eigenvector-based device-free passive localization using array sensor," *IEEE Trans. Veh. Technol.*, vol. 64, no. 4, pp. 1354–1363, Apr. 2015.

[9] L. M. Ni, D. Zhang, and M. R. Souryal, "RFID-based localization and tracking technologies," *IEEE Wireless Commun.*, vol. 18, no. 2, pp. 45–51, Apr. 2011.

[10] H. Qin, Y. Peng, and W. Zhang, "Vehicles on RFID: Error-cognitive vehicle localization in GPS-less environments," *IEEE Trans. Veh. Technol.*, vol. 66, no. 11, pp. 9943–9957, Nov. 2017.

[11] W. Ruan *et al.*, "Tagtrack: Device-free localization and tracking using passive RFID tags," in *Proc. 11th Int. Conf. Mobile Ubiquitous Syst.*, London, U.K., 2014, pp. 80–89.

[12] J. Shen, A. F. Molisch, and J. Salmi, "Accurate passive location estimation using TOA measurements," *IEEE Trans. Wireless Commun.*, vol. 11, no. 6, pp. 2182–2192, Jun. 2012.

[13] Y. Wang, S. Ma, and C. P. Chen, "TOA-based passive localization in Quasi-synchronous networks," *IEEE Commun. Lett.*, vol. 18, no. 4, pp. 592–595, Feb. 2014.

[14] W. Yuan *et al.*, "Expectation-maximization-based passive localization relying on asynchronous receivers: Centralized versus distributed implementations," *IEEE Trans. Commun.*, vol. 67, no. 1, pp. 668–681, Jan. 2019.

[15] N. Decarli, F. Guidi, and D. Dardari, "A novel joint RFID and radar sensor network for passive localization: Design and performance bounds," *IEEE J. Select. Areas Commun.*, vol. 8, no. 1, pp. 80–95, Feb. 2014.

[16] X. Zhang, H. Li, J. Liu, and B. Himed, "Joint delay and doppler estimation for passive sensing with direct-path interference," *IEEE Trans. Signal Process.*, vol. 64, no. 3, pp. 630–640, Feb. 2016.

[17] K. Keykhosravi and H. Wymeersch, "Multi-RIS discrete-phase encoding for interpath-interference-free channel estimation," 2021. [Online]. Available: https://arxiv.org/abs/2106.07065

[18] S. M. Kay, *Fundamentals of Statistical Signal Processing: Estimation Theory*. Englewood Cliffs, NJ, USA: Prentice Hall PTR, 1993.

[19] M. Malanowski, "An algorithm for 3D target localization from passive radar measurements," in *Proc. SPIE-Photon. Appl. Astron., Commun., Industry, High-Energy Phys. Exp.*, Wilga, Poland, vol. 7502, May 2009, pp. 75021B-1–75021B-6.

[20] S. W. Ellingson, "Path loss in reconfigurable intelligent surface-enabled channels," 2019, *arXiv:1912.06759*.

Authorized licensed use limited to: Universitat Autonoma De Barcelona. Downloaded on July 19,2022 at 23:51:31 UTC from IEEE Xplore. Restrictions apply.